Journal of Electroanalytical Chemistry 839 (2019) 123–133

Contents lists available at ScienceDirect

Journal of Electroanalytical Chemistry

journal homepage: www.elsevier.com/locate/jelechem

Photoelectrochemical degradation of bisphenol A using Cu doped WO_3 electrodes

Lorena Athie Goulart, Suellen Aparecida Alves, Lucia Helena Mascaro*

Universidade Federal de São Carlos, Rodovia Washington Luiz, km 235, São Carlos, SP, Brazil

ARTICLE INFO

Keywords:
Bisphenol A
Cu doped WO_3
Photodegradation
Visible light activity
Intermediates
Electrochemical sensor

ABSTRACT

Cu-doped WO_3 electrode was fabricated on FTO substrate via one step preparation by modified sol-gel method using a suspension of $[(NH_4)_{10}H_2(W_2O_7)_6]$ and $CuSO_4{\cdot}5H_2O$ in mix of polyethylene glycol 300 and ethylene glycol. Photoelectrocatalytic degradation of bisphenol A (BPA) with Cu-doped WO_3 electrode was performed under visible light irradiation and H_2O_2 as auxiliary oxidizing agent. For monitoring of the photoelectrocatalysis it was used conventional and alternative method (UV–Vis spectrophotometry and electrochemical sensor, respectively). After 8 h of assay, it was verified removal of 80% of BPA and formation of the phenolic intermediates using electrochemical sensor and 75% of total carbon organic removal.

1. Introduction

Reduction of environmental pollution and especially the growing demand for potable water is one of the most serious challenges worldwide. Besides the shortage of water resources, the presence of toxic chemicals, even at extremely low concentrations, such as endocrine disrupters can causes potential risk to the environment and human health. The endocrine disruptors are able to alter the natural functioning of the endocrine system, may cause different types of cancer and harm the reproductive systems of the affected beings [1]. The main sources of estrogens at the aquatic environment are domestic sewage, which contains the female hormone excretion, hospital wastewater and manufacturing plants effluents [2].

Bisphenol A (BPA) is an organic compound identified as an endocrine disrupter, and is used in large quantities in paints, plastics and epoxy resins industry. BPA is found in the environment as a result of leaching process of manufactured end products besides being present in household products and pharmaceutical formulations [3]. Many researches are developing biochemical and physicochemical advanced methods to eliminate BPA from water sources, since this product may cause serious damage to the environment, to human and animals [4].

Among the methods used in the degradation of emerging pollutants, heterogeneous photocatalysis has excelled in recent years due to its high mineralization efficiency, low toxigenicity and possibility to use of light sun at the process [5]. This method is based mainly on the in situ generation of hydroxyl radicals under ambient conditions that are capable of converting various toxic organic compounds, including non-biodegradable, in end products such as CO_2, H_2O and inorganic mineral ions [6].

Various materials have been used as photocatalyst for the degradation of BPA [7–10]. The tungsten oxide (WO_3) is an important *n*-type semiconductor that has received great attention due to its ability to absorb in the visible light region. Besides this, it is an inexpensive material with high stability in aqueous solutions under acidic conditions, it does not submit to photocorrosive process and exhibits polymorphism [11]. WO_3 has been applied in smart windows, solar energy conversion, storage cells, solar cells of water-splitting, gas sensors, electrochromic and photochromic devices, secondary batteries and photocatalysts [12–18].

Several investigations have been made in recent years in the application of the WO_3 as a photocatalyst, due to its relatively narrow energy band-gap (< 3.0 V) [19]. The transition metals are highlighted in electrocatalysis due to the presence of unpaired electron and orbital *d* unfilled, forming ties with adsorbates [20]. However, the WO_3 alone exhibits very low catalytic activity under irradiation of visible light. Thus, several attempts have been made to improve the photocatalytic activity of the WO_3. Co-catalysts such as platinum, gold, and silver, have been used to increase the photoactivity of the WO_3 [21–24].

Oxides and metal ions have also been studied for improving the photocatalytic activity of the WO_3. Composites made of WO_3 and different oxides such as $CuBi_2O_4$ [25], $CaFe_2O_4$ [26], TiO_2 [27] and CuO [28] were prepared and used as photocatalysts. The addition of Cu and Cu ions as co-catalysts on the WO_3 surface was also made [29]. It was verified that a simple mixture of CuO and $CuBi_2O_4$ with WO_3 to create

* Corresponding author.
E-mail address: lmascaro@ufscar.br (L.H. Mascaro).

https://doi.org/10.1016/j.jelechem.2019.03.027
Received 20 September 2018; Received in revised form 7 February 2019; Accepted 13 March 2019
Available online 14 March 2019
1572-6657/

an efficient photocatalyst for decomposing volatile gas and addition of Cu (II) on WO_3 surface causes a significant improvement in the visible light photocatalytic oxidation of organic compounds. Copper compounds have been widely used because they can contribute to the O_2 reduction process, and may extend the length of light absorbed from the UV to the visible region due to the adjustment of the conduction band edges of both CuO and CuO_2 which are −0.96 and −0.22 V, respectively [30].

WO_3 and Cu are extensively used in the degradation of organic pollutants due to its unique properties. However, there are no reports in the literature that shows these compounds in a combination assays for photocatalytic degradation of BPA. Therefore, WO_3 doped with Cu film electrodes have been developed and applied in the BPA photodegradation and the results were promising.

A current challenge at monitoring in organic degradation process is the development of analytical methods capable of identifying a pollutant with high sensitivity and low detection limit. In general, the degradation monitoring is carried out by high performance liquid chromatography (HPLC) which require a great demand for time and reagents, which is not recommended according to the principles of green chemistry. So, in addition to spectroscopic techniques, in this work, of the BPA photocatalytic degradation and the formation of intermediates was accompanied using an electrochemical sensor.

Thus, this study presents as the goal of evaluating the photoelectrochemical degradation of the emerging pollutant BPA with Cu-doped WO_3 electrode under solar energy simulated and the monitoring of the degradation using spectrophotometry, electrochemical sensor and total organic carbon.

2. Experimental

2.1. Reagents

All reagents were analytic grade and were used as raw materials without further purification. Ammonium tungstate $[(NH_4)_{10}H_2(W_2O_7)_6]$ (99.99% Sigma-Aldrich), polyethylene glycol 300 (PEG 300, Sigma-Aldrich), ethylene glycol (EG, 99.8% Sigma-Aldrich), hydrated copper sulphate ($CuSO_4{\cdot}5H_2O$, 98–102%, Reagen), sodium sulphate (Na_2SO_4, 99.0%, J.T. Barker), bisphenol A (BPA, ≥99%, Sigma- Aldrich) and hydrogen peroxide (H_2O_2, 29.0%, Synth). Phosphate buffer solution (PBS) (0.1 mol L^{-1}) was prepared using NaH_2PO_4 and Na_2HPO_4 (Synth). The pH of the buffer solution was adjusted using NaOH (Synth). All aqueous solutions were prepared with water purified from a Millipore Milli-Q system (> 18.2 MΩ).

2.2. Synthesis of WO_3 and Cu doped WO_3 electrodes

The WO_3 and Cu doped WO_3 thin films were prepared by synthesis method developed by the our research group [31]. The precursor used was $(NH_4)_{10}H_2(W_2O_7)_6$ dissolved in a mixed of EG + PEG 300 (1:4 v/v) with final concentration of 0.03 mol L^{-1}. The white suspensions obtained were deposited on the FTO substrate by drop casting method (5 μL cm^{-2} and total area of 1.5 cm^2). Each layer deposited was dry at 170 °C and the calcination was carried out at 500 °C for 5 h in air atmosphere (heating rate: 170–270 at 1 °C min^{-1} keeping at 270 °C during 20 min and 270–500 °C min^{-1} at 5 °C min^{-1} keeping at 500 °C during 5 h). Cu doped WO_3 films were prepared by similar procedure, but in the suspension preparation was added $CuSO_4{\cdot}5H_2O$ in the proportions of 0.5; 1.0; 1.5 and 2.0% (w/w). Then, the electrodes were designed by W_0 (undoped), $CW_{0.5}$, $CW_{1.0}$, $CW_{1.5}$ and $CW_{2.0}$, respectively (Scheme 1). Fig. 1 shows a schematic diagram of confection of the electrodes.

2.3. Morphology and structural characterization techniques

The structure characterization was carried out by powder X-ray diffraction using a XRD 6000 Shimadzu diffractometer with Cu Kα radiation. The X-ray diffraction data of the samples were collected in the 2θ range of 10–60°. The morphology study of WO_3 and Cu doped WO_3 films were carried out by field emission scanning electron microscopy (ESEM-FEG, FEI Inspect F 50). The amount of Cu in each doped film was measured by microanalysis using an energy dispersive X-ray spectroscopy (EDAX, EDX-GENESIS). UV-diffuse reflectance spectra of the samples were measured by using a UV–Vis spectrophotometer (Shimadzu UV spectrophotometer).

2.4. Photoelectrochemical characterization

Cyclic voltammetry (CV) measurements were performed in 0.5 M Na_2SO_4 as electrolyte, a platinum plate as the counter electrode, WO_3 and Cu doped WO_3 as the working electrode and Ag/AgCl/KCl saturated as reference electrode. The potential sweep was performed at range of 0.0 and 1.5 V and of scan rate 20 mV s^{-1}. The photoelectrocatalytic activity of the electrodes was measured using a simulated AM1.0 illumination (100 W) with a Newport Sol3A Class AAA solar simulator. All films were illuminated with light from the front and backside.

2.5. Degradation assays

The BPA photoelectrocatalytic oxidation was carried out in a glass cell equipped with a working electrode ($CW_{1.0}$), an auxiliary electrode of Pt and a reference electrode of Ag/AgCl/KCl saturated. The measurements were made in 200 mL of 0.5 mol L^{-1} Na_2SO_4 solution. The photoactive area of the $CW_{1.0}$ anode was 1.5 cm^2 and it was illuminated with Vapour Metallic Lamp (HQI-TS Osram, 150 W). The experiments were made inside of a black box to avoid interference of external lighting. An Autolab PGSTAT30 model (Eco Chemie, Utrecht, Netherlands) potentiostat/galvanostat, controlled by GPES 4.9 software (Eco Chemie) was used at the photoelectrocatalytic oxidation measurements. Firstly, current applied during electrolysis was 5 mA cm^{-2} and the pH of solutions was not adjusted. Aliquots of the samples of BPA solution were withdrawn at regular time of 0, 30 and 60 min and the progress of photoelectrodegradation of BPA was monitored by absorbance measurements in a UV–Vis spectrophotometer (Shimadzu UV spectrophotometer) operating from 200 to 800 nm in a quartz cell. The effects of experimental conditions on the photoelectrodegradation of BPA such the initial concentration of BPA, pH of solution, applied current density, and H_2O_2 concentration was studied. Exhaustive electrolysis was made to study intermediates formed during the degradation of BPA. In addition, total organic carbon was monitored by a total organic carbon analyzer (Sievers InnvOx Laboratory Total Organic Carbon).

2.6. Electrochemical monitoring of intermediates

A new form to monitor the degradation of BPA and the intermediates formed during photoelectrolysis was applied in this work. The decay of the concentration of the BPA and the formation of intermediates were monitored by an electrochemical sensor. The sensor used was developed by our research group and consist in a glassy carbon electrode modified with nickel oxide nanoparticles and carbon nanotubes (NiO/MWCNT/GCE) [32]. During electrolysis, aliquots of the sample of BPA solution were withdrawn at regular time and diluted in 0.1 mol L^{-1} PBS solution pH 6.0 to electrochemical analysis. The measurement was carried out in a conventional three-electrode cell with NiO/MWCNT/GCE as the working electrode, Ag/AgCl (KCl 3.0 mol L^{-1}) as the reference electrode and platinum as the counter electrode. Cyclic voltammetry (CV) experiments were carried out in a potential range from −0.2 V to +1.0 V with a scan rate of 50 mV s^{-1}. Each scan, the electrode was subjected to an electrochemical treatment to renew its surface, where −0.8 V was applied for 100 s and then it

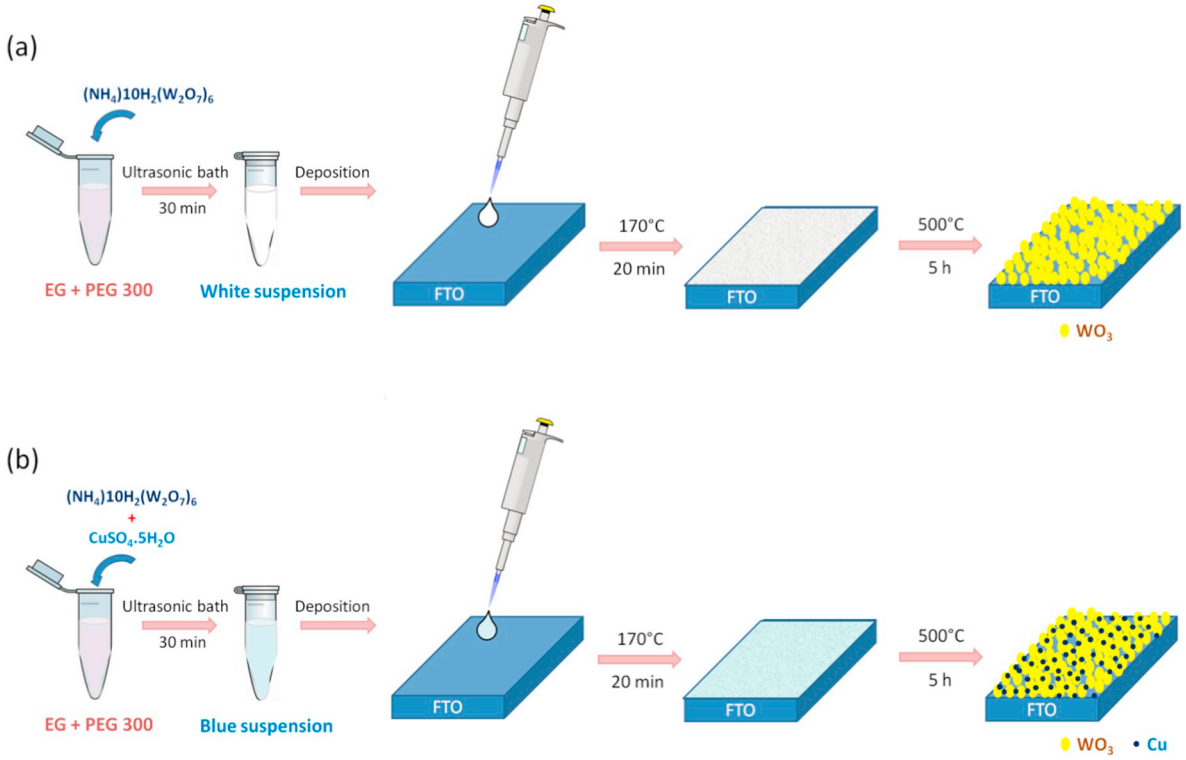

Scheme 1. Schematic diagram of manufacture of WO_3 and Cu doped WO_3 electrodes.

was cycled 10 times in PBS solution pH 7.0.

3. Results and discussion

3.1. Morphologic, structural and optical characterization

Morphology and particle size of films were investigated by SEM-FEG. Fig. 1(a–e) shows images obtained to film without Cu and doped with Cu in the nominal proportion of 0.5; 1.0; 1.5 and 2.0%, respectively. It is observed that the substrate is recovery completely all electrodes with dense films which present grains homogenously distributed. This morphology is similar to films prepared form others methods [33,34]. An important characteristic is the porosity of the films, which is achieved by PEG presence. This organic polymer promotes high adherence of the film and high porosity. It was not observed significant difference in the morphology of films with Cu presence. Grain diameters were estimated by microscopy analysis as well and Table 1 show diameter ranging from 30 to 50 nm to each film deposited. The thickness of film deposited was valued according to Fig. 1f. Each deposited layer presents thickness of 860 nm after calcination. This result is very important because very thick films are subject to higher recombination of the pair electron/hole when illuminated by light.

Semiquantitative analysis was performed by EDX and the composition of the films after the annealing process is presented in Table 1. The amounts of Cu added vary from 0.5 to 2% by weight relative to the concentration of ammonium tungstate as the precursor. It was observed that from 1.5% Cu it is not possible to add more dopant, and the percentage reaches a maximum of 1.1%. From this percentage, the Cu may have reached an optimum doping concentration and the excess may be present in other non-doped forms. Average atomic percentages (at.%) confirm that the main elements found in the samples were oxygen and tungsten with respect to 3 oxygen atoms to 1 of tungsten in all the films.

The mapping results showed that the elements W, O and Cu were distributed homogeneously throughout the film without presence of Cu agglomerates (Fig. 1g). This behavior was observed to all electrodes with different doping levels. Thus, the synthesis method used to produced WO_3 electrodes doped with Cu in one step it was carried out successfully and homogeneous films were produced.

To analyze crystallinity of the films, X-ray diffractograms (XRD) of the WO_3 and Cu-doped WO_3 films were measured in the range of $10^\circ \leq 2\theta \leq 60^\circ$ with a rate of 1° per minute (Supplementary data, Fig. A2). The major peaks for monoclinic WO_3 were present at 23.3°, 23.7°, and 24.4°, which correspond to the (002), (020), and (200) planes, respectively (PDF No. 43-1035). Moreover, it is noted other diffraction peaks which can be associated to FTO substrate (SnO_2, PDF No. 88-287). No peak should be related to Cu presence. This can be associated by small amount of Cu deposited and the addition of Cu ion into the W lattice site rather than interstitial ones. Similar results were observed with the doping of Cu in other semiconductors like TiO_2 and ZnO. The characteristic peaks of Cu at the ZnO nanoparticles only was observed at the X-ray diffractograms with a Cu content > 15% [35–37].

WO_3 presents relatively wide band gap energy (2.6–3.0 eV) and it is excited by the blue and near ultraviolet regions of the solar spectrum. To increase the photocatalytic performance it is possible decrease the band gap and thus, the material will be activated in region closer to the visible of the solar spectrum, what is interesting of point view of application of this material since this region is the most abundant. To verify the band gap energy of the electrodes WO_3/FTO and Cu-doped WO_3/FTO were performed diffuse reflectance measurements (Supplementary data, Fig. A3.a).

The optical bang gap determination was carried out from Tauc plot and Kubelka-Munk unit. The Kubelka–Munk unit of absorption is calculated by follow equation: [38].

$$F(R) = \frac{(1-R)^2}{2R} \quad (1)$$

where R is reflectance and F(R) is the absorbance (Fig. 2a). All electrodes showed radiation absorption in the range of 300–450 nm. Maximum doped electrode presented a slight shifting in the absorption band to the visible region. Moreover, it is noted two additional absorption: first absorption between 450 and 500 nm and second one between 550 and 800 nm. The first absorption can be associated to charge transfer

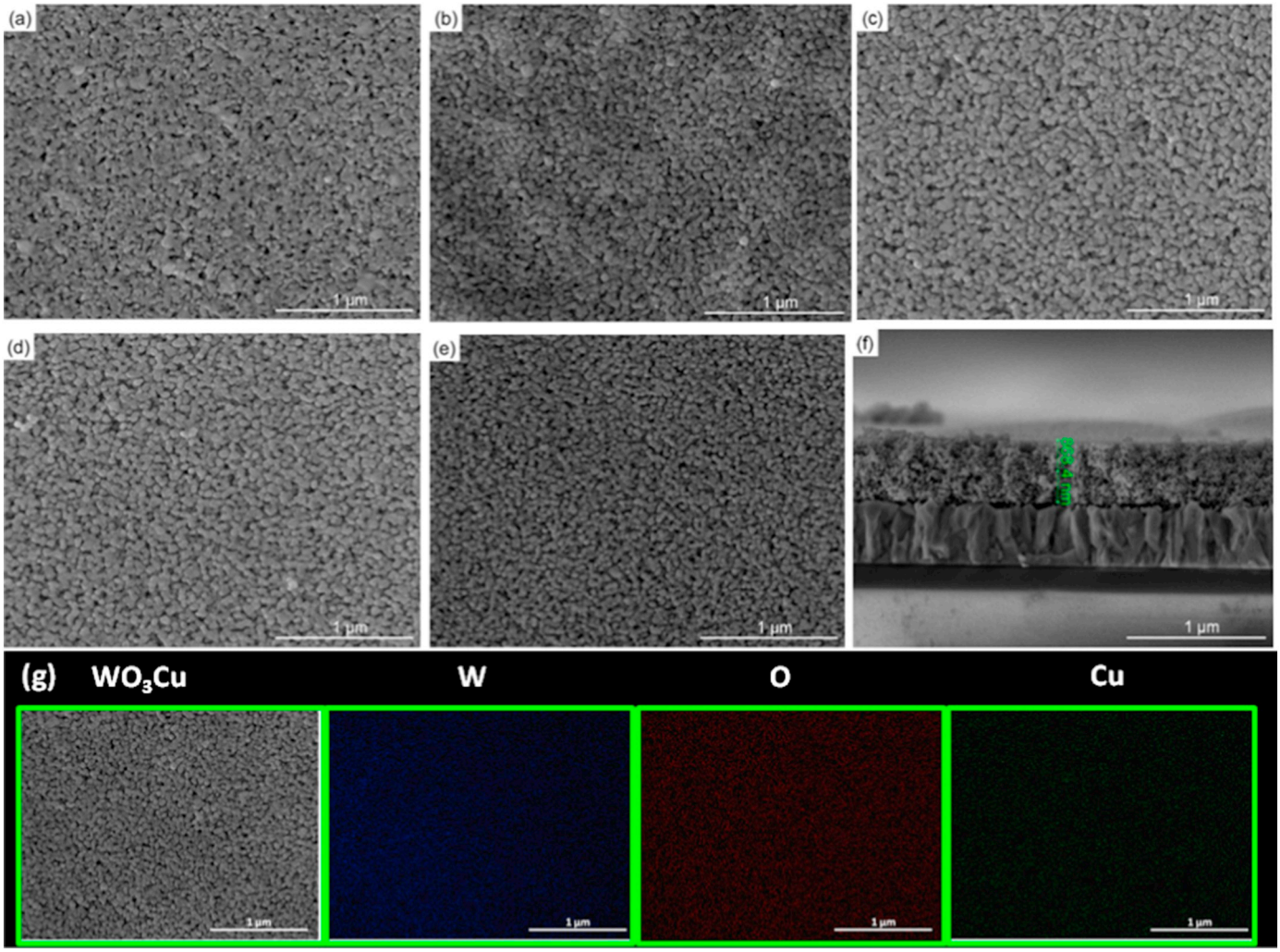

Fig. 1. Scanning electron microscopy images of WO_3 films deposited after calcination: (a) W_0; (b) $CW_{0.5}$, (c) $CW_{1.0}$, (d) $CW_{1.5}$, (e) $CW_{2.0}$, (f) image of W_0 electrode cross section and (g) SEM-EDX mapping of the $CW_{1.0}$.

Table 1
Estimated particle diameter, composition and optical properties of WO_3 and Cu doped WO_3 electrodes.

Electrode	Nominal Cu amount (%)	Particle diameter (nm)[a]	Cu amount[b] (wt%)	Band gap Eg (eV)
W_0	0.0	30 ± 2.32	–	2.97
$CW_{0.5}$	0.5	50 ± 6.08	0.3	2.96
$CW_{1.0}$	1.0	35 ± 2.33	0.9	2.96
$CW_{1.5}$	1.5	40 ± 5.20	0.8	2.94
$CW_{2.0}$	2.0	40 ± 5.20	1.1	2.78

[a] By SEM analysis.
[b] By EDX analysis.

from O (from WO_3) 2p to Cu(II) as clusters or CuO [39,40]. The second absorption can be attributed to d-d transition of Cu(II) presents in the crystalline WO_3. This absorption increases according to doping level [39].

The bang gap was estimated by plot of $[F(R)h\nu]^n$ against $h\nu$. This value is obtained when $[F(R)h\nu]^n$ vs. $h\nu$ is equal to zero. It is considered the WO_3 as a direct band gap semiconductor, then $n = 2$. The band gap determination curves for all electrodes are shown in Fig. 2 and the values obtained of band gap energy can be observed in Table 1.

Indeed, the Cu amount is too small to promote significative changes in band gap energy. Until the doping of 1.5% of Cu, the band gap values are very similar and they are agreement with expected value to WO_3 monoclinic phase [41]. However, $CW_{2.0}$ electrode, i.e. more doped electrode, presented the band gap value of 2.78 eV. This value of band gap corresponds to shifting in the absorption to visible region compared to not doped WO_3.

3.2. Photoelectrochemical behavior of WO_3 and Cu doped WO_3 electrodes

The electrochemistry characterization of the electrodes is needed to verify the effect of doping in relation to the photocurrent of the synthesized electrodes. It was evaluated the photoelectrocatalytic activity of Cu-doped WO_3 by electrochemical measurements in light presence using a solar simulator (Supplementary data, Fig. A1.a). It was observed the dopant effect in photoelectrochemical assays. The photocurrent increases with Cu presence to all electrodes. There is a slight increase in photocurrent response with Cu- doped WO_3 0.5%, with three times more photocurrent than WO_3 undoped electrode. For comparison effect, it was chosen the potential of +0.71 V vs Ag/AgCl at pH 5, which corresponds to the thermodynamic potential for water oxidation. The dopant percentage of 1.0% presented the higher photocurrent response, with 87 µA cm^{-2}, then the photocurrent increase at six times compared to WO_3 not doped electrode. When the doping level is extended to 1.5 and 2%, the photocurrent response decreases again but values are higher than 0.5% and not doped electrode. This behavior it was expected because according elemental analysis (EDX), from 1.0% is not possible adding more dopant efficiently in WO_3. From photocurrent

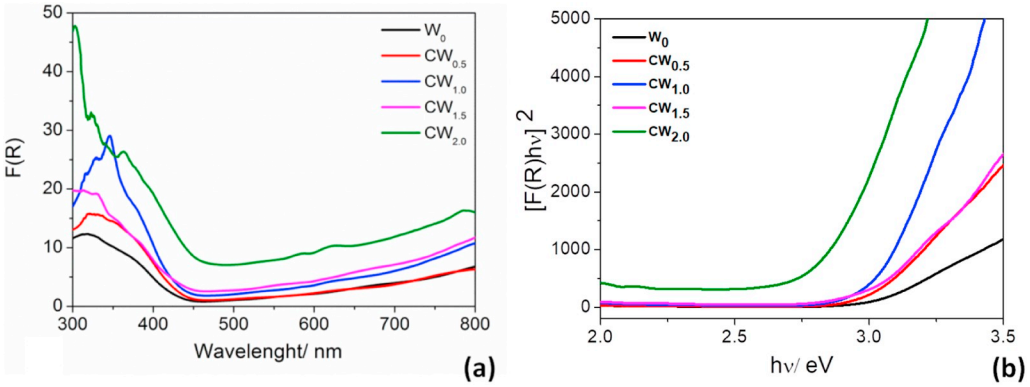

Fig. 2. Kubelka-Munk absorption curves of WO_3 and Cu doped WO_3 electrodes (a) and determination of band gap of W_0, $CW_{0.5}$, $CW_{1.0}$, $CW_{1.5}$ and $CW_{2.0}$ electrodes (b).

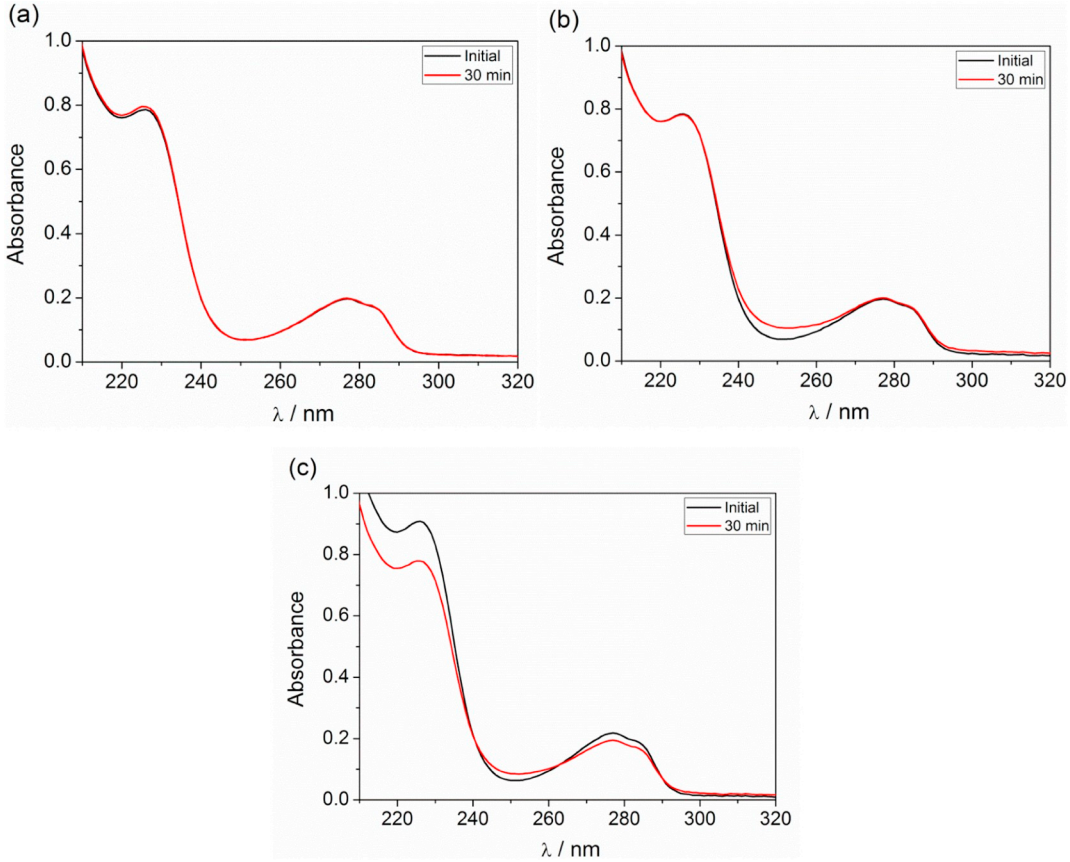

Fig. 3. UV–Vis absorption spectra at 30 min of oxidation 60 ppm of BPA in 0.5 mol L^{-1} Na_2SO_4 (a) photocatalysis (light irradiation), (b) electrolysis (5 mA cm^{-2}) and (c) photoelectrocatalysis (light irradiation + 5 mA cm^{-2}); vapour metallic lamp 150 W.

results, it was chosen the electrode with 1.0% of Cu to degradation study.

In addition, it was evaluated the number of layers of precursor suspension in photoelectrochemical response in Na_2SO_4 0.5 M (Supplementary data, Fig. A1.b). Clearly, it was noted that the number of layers affect the photocurrent values. When it is deposited just one layer of precursor suspension, it is reached the higher photocurrent compared to others electrodes with different layers. With 2 and 4 layers it is obtained the same behavior with same photocurrent. The electrode with 3 layers presented the minor photocurrent response of all electrodes. After 4 deposited layers, it is not possible a film with quality, i.e., with homogeneity and small thickness. From photocurrent results, it was chosen the electrode with 1.0% of Cu and 1 layer to degradation study.

3.3. Photochemical, electrochemical and photoelectrochemical oxidation of the BPA

The efficiency of photoelectrochemical degradation (light irradiation and current density applied, 5 mA cm^{-2}) in relation to photochemical (light irradiation) and electrochemical (5 mA cm^{-2}) to sample content 60 ppm of BPA in 0.5 mol L^{-1} Na_2SO_4 was evaluated. The process was monitored after 30 min of oxidation by measurement absorbance decay at $\lambda = 276$ nm. During BPA oxidation, the maximum absorbance diminishes in 13% after treatment using photoelectrocatalysis. However, it was not observed decrease at BPA absorbance band at when photocatalysis and electrolysis was used to perform the oxidation, as show in Fig. 3.

The results clearly indicated that the light irradiation and the

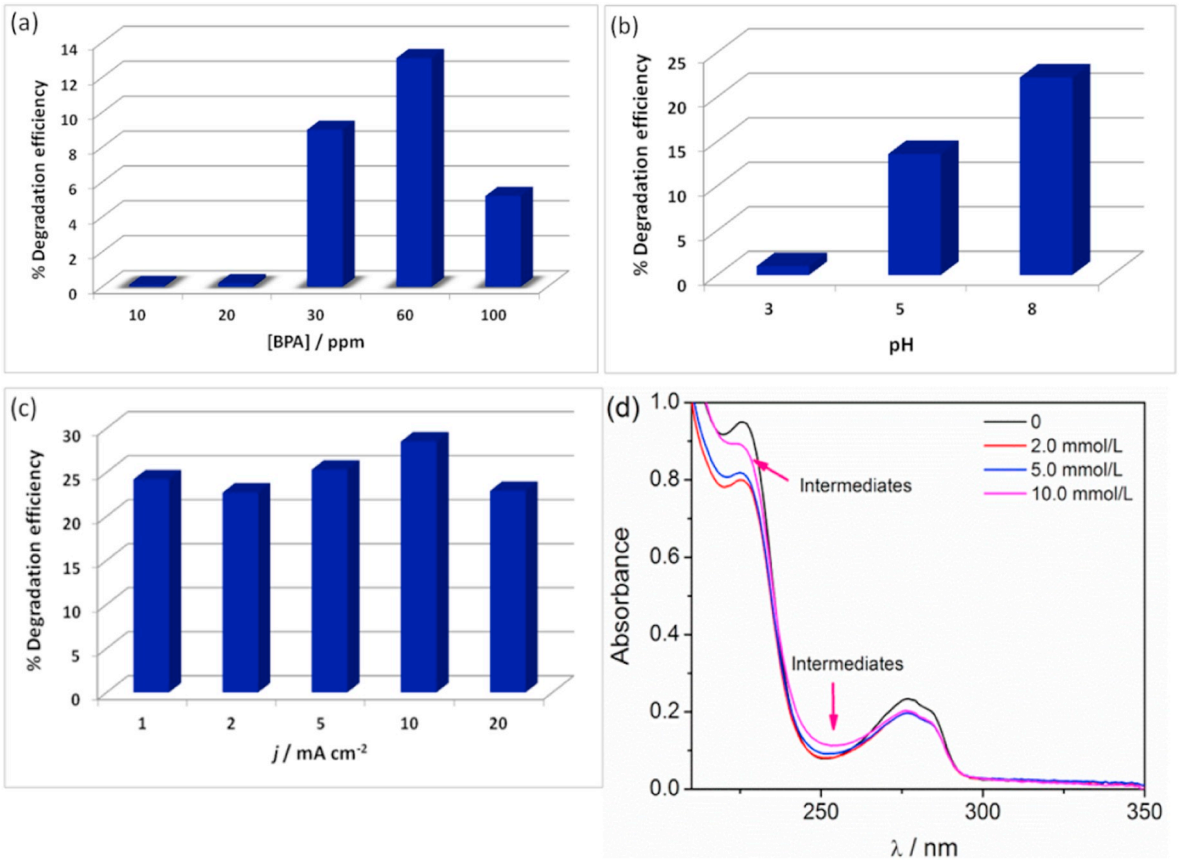

Fig. 4. Effects of experimental conditions on the photoelectrodegradation of BPA: (a) initial concentration of BPA, (b) pH, (c) applied current density and (d) H_2O_2 concentration; vapour metallic lamp 150 W.

current used alone were not efficient to degrade of BPA. However, the combination of light irradiation and current in the photoelectrocatalytic experiments were more effective to promote the decay of BPA absorption band in just 30 min.

3.3.1. Optimization of degradation parameters in photoelectrochemical process

The synergism between photo and electrochemical processes is needed to degrade the pollutant BPA. Thus, some parameters were studied to evaluate the efficiency of the degradation process of BPA, which are: initial concentration of BPA, pH, applied current density and amount of auxiliary oxidizing agent, H_2O_2.

The influence of the initial concentration of BPA at the photoelectrocatalysis experiments was investigated evaluating solutions of 0.5 mol L^{-1} Na_2SO_4 containing 10, 20, 30, 60 and 100 ppm of BPA. The degradation efficiency was monitored at the 30 min of oxidation by measurements of absorbance decay at $\lambda = 276$ nm. At the Fig. 4a can be observed the percentage of degradation versus BPA concentration. Increasing BPA concentration from 10 to 20 ppm has practically no effect on absorbance decay band, while a further increase from 20 to 30 ppm results in 9% of degradation and 14% was observed with 60 ppm. Higher concentrations decrease the degradation efficiency percentage of BPA. Studies show that the degradation performance will be dictated by the catalyst sites to substrate molecules ratio. At low BPA concentrations, in the range 10 to 30 ppm at the experimental conditions of this study, catalyst sites at the $CW_{1.0}$ anode are in excess and they can accommodate all BPA molecules. However, in very low concentrations, less analyte reaches the surface of the electrode and the free radicals formed in the photocatalytic processes and that would aid in the degradation of the BPA, can recombine, thus reducing its degradation.

This behavior is illustrated in Scheme 2a. The decreases of degradation of BPA at high initial concentrations as 100 ppm for example, may be explained by (i) an increase of the molar extinction coefficients due the formation of numerous reaction intermediates at high concentrations, thus absorbing a considerable portion of the emitted radiation, and (ii) less active sites are accessible at higher BPA concentrations, thus triggering a competitive adsorption onto the catalyst surface, which in that way decreases the formation of OH· and $O_2\cdot^-$ free radicals attacking BPA and photodegradation efficiency (Scheme 2b) [42,43].

The effect of the initial pH on the BPA photoelectrodegradation for the $CW_{1.0}$ anode is shown in Fig. 4b. It can be seen that BPA degradation efficiency % increased with increasing of initial pH. Specially, 1%, 13% and 22% of degradation were observed at initial values pH of 3, 5 and 8, respectively. The photoelectrocatalysis is much faster under alkaline conditions; however, above pH 11 occurred a reduction of the photocatalytic activity and a decrease of degradation efficiency (data not shown). The effect of initial pH at the BPA photodegradation can be explained as a consequence of the electrostatic interactions and the pK_a value of molecule. In highly acid and alkaline conditions, such pHs 3 and 11, the low photodegradation rates recorded may be due to the adsorption capacity of BPA associated with the electrostatic interactions between BPA and the charged semiconductor surface. At higher pH values, repulsion will occur between BPA and catalyst because both are negatively charged, while at lower pH, due BPA is not charged and the attraction on the catalyst surface is difficulties. Additionally, BPA molecule has two ionizable hydrogen atoms with pK_a of 9.6–10.2 and this implies the BPA is in the ionized form, as bisphenolate anions (BPA^- and BPA^{2-}) at pH values close to 10 [43]. Therefore, at the higher pH the molecule could be more readily attacked by the electrophilic OH· radical than lower pH values. In addition, the increased

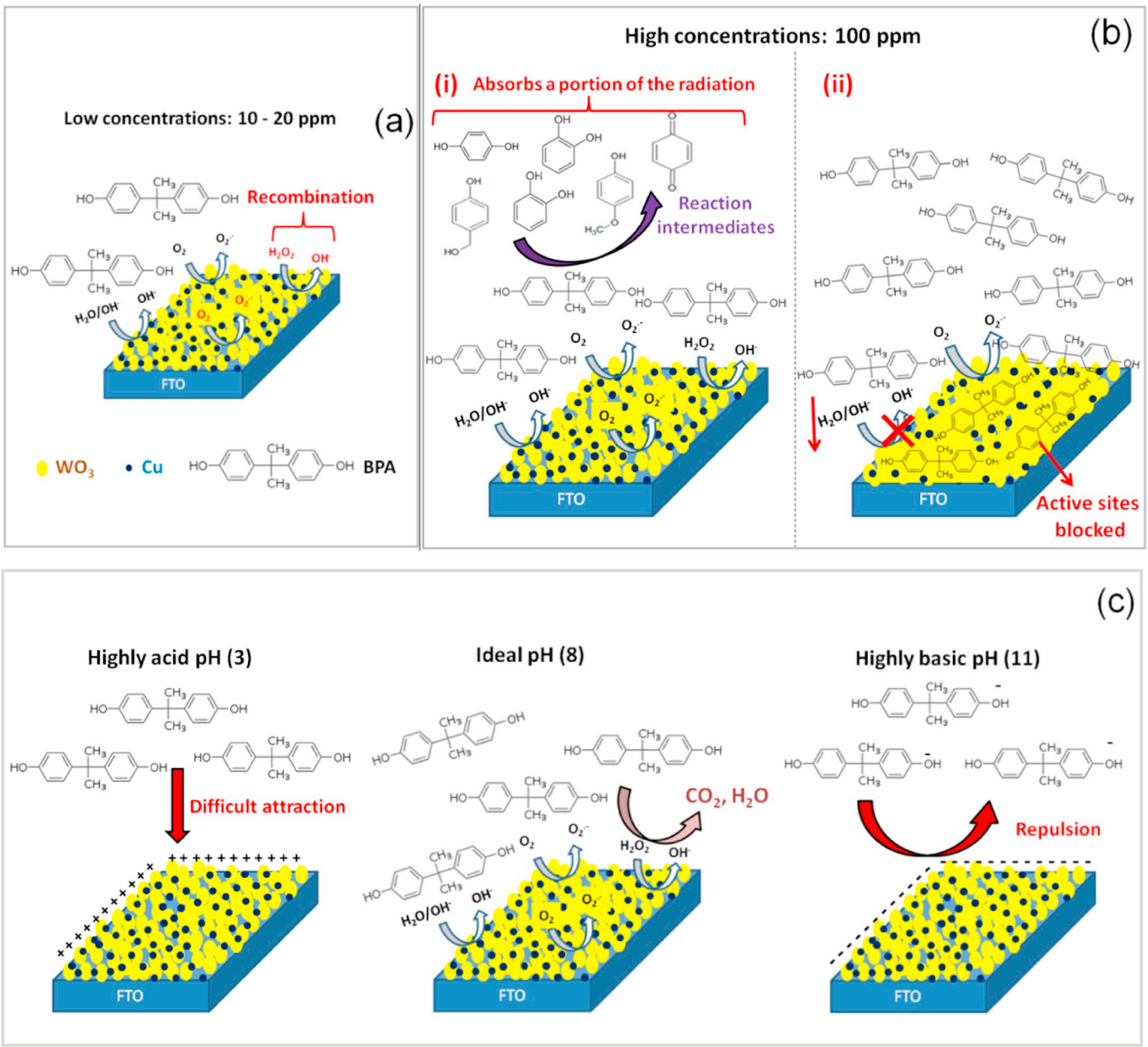

Scheme 2. Illustration of the photoelectrolysis of the BPA with $CW_{1.0}$ anode in different conditions: (a) 10–20 ppm of BPA; (b) 100 ppm of BPA and (c) different initial pH values.

performance recorded at pH 8 may partly be due to the fact that hydroxyl radical formation is favoured at alkaline conditions [44,45]. The Scheme 2c illustrates the interaction between BPA and CW1.0 anode in different initial pH values.

The effect of current density (*j*) on the electrochemical degradation of BPA in the range 1–20 mA cm^{-2} is shown in Fig. 4c. As can be seen lower *j* (1, 2 and 5 mA cm^{-2}) result in approximately 25% of decay absorbance of BPA and 10 mA cm^{-2} promote 28% of degradation after just 30 min of reaction. At 20 mA cm^{-2} was observed decrease of removal of BPA which may be attributed to higher formation of oxygen in surface of electrode that can decrease the catalyst sites. In addition, in this *j* there was the removal partially of films of CW1.0 at the surface of FTO. These results show that 10 mA cm^{-2} would be a great bias to promote enough potential to the flat band potential to more separate charges by removing electrons to the cathodes. Generally, to BPA degradation are used higher currents densities than used in this work [46]. Titanium electrodes modified with platinum (Ti/Pt) and tin oxide (Ti/SnO_2) completely degraded the BPA by applying a current density of 300 mA cm^{-2} [47]. Titanium electrodes and boron doped diamond (Ti/DDB), titanium with tin oxide and antimony (Ti/Sb-SnO_2) films, titanium and ruthenium oxide (Ti/RuO_2) and platinum electrode (Pt) mineralized BPA by applying 50 mA cm^{-2} for 10 h [48]. Anodes of titanium modified with tin oxide (Ti/SnO_2), iridium oxide (Ti/IrO_2) and lead oxide (Ti/PbO_2) were applied in the electrolysis of BPA and required 2.0 A cm^{-2} to degrade 90% of BPA in solution [49].

In this way, the developed anode in this work is very promissory to be used in the BPA photodegradation in consequence of its high photocatalytic activity mainly at the first minutes of reaction, using current densities lower than previously reported.

The addition of H_2O_2 significantly improves the photocatalysis efficiency due it may accept photogenerated electrons by [50]:

$$H_2O_2 + e^- = OH\bullet + OH^- \quad (2)$$

$$H_2O_2 + h\nu = 2OH\bullet \quad (3)$$

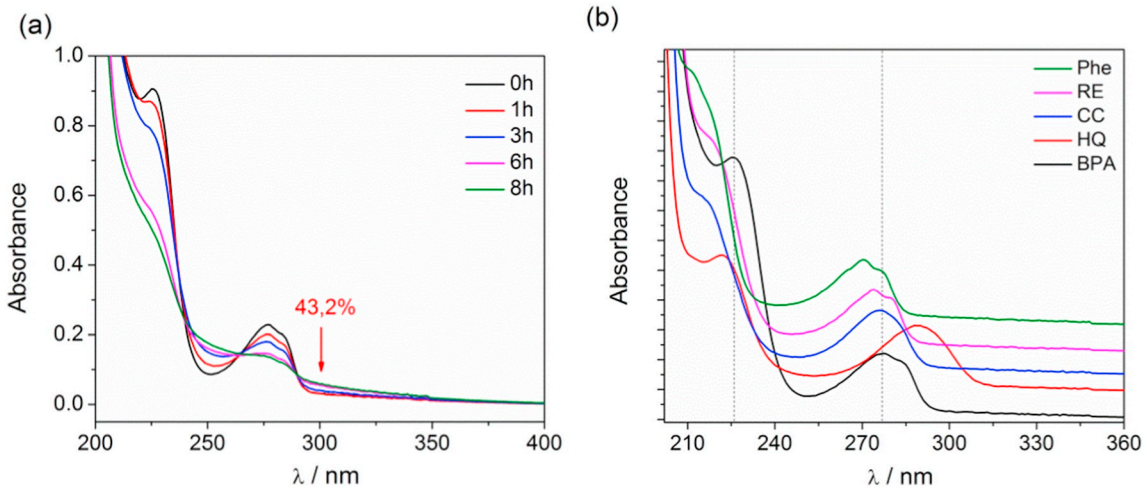

Fig. 5. (a) UV–Vis absorption spectra at different times under optimal conditions and (b) UV–Vis absorption spectra of phenol (Phe), resorcinol (RE), catechol (CC), hydroquinone (HQ) and bisphenol A (BPA).

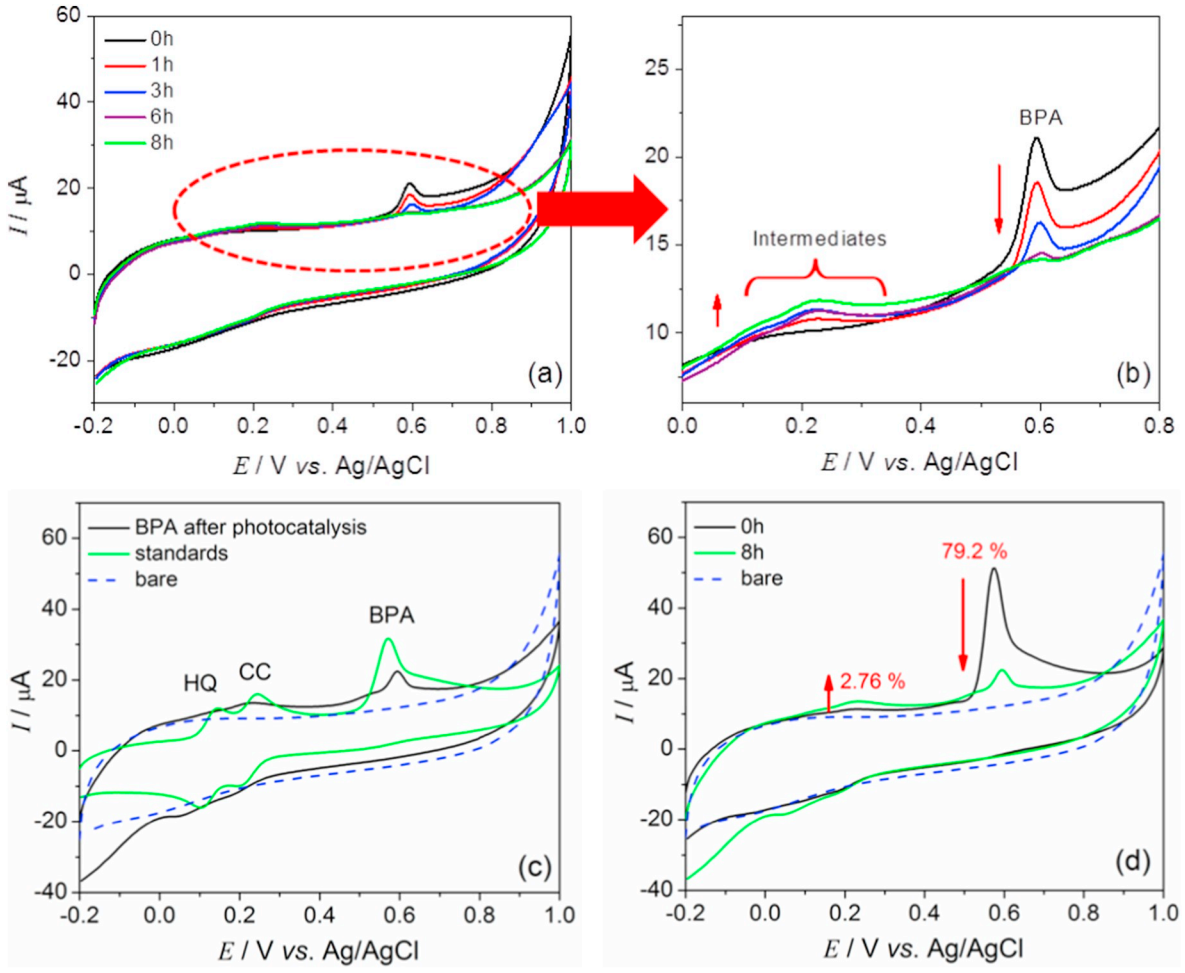

Fig. 6. CVs at NiO/MWCNT/GCE in 0.1 mol L^{-1} PBS (pH 6.0) (a) at different times of photocalysis of BPA; (b) details of graph (a).; (c) CV of a solution containing BPA, HQ and CC and CVs obtained in time of 8 h of degradation of BPA and (d) initial and final voltammograms in less diluted samples.

The photo-Fenton oxidation generates hydroxyl radicals to oxidize numerous contaminants when H_2O_2 is reacted with transition metal as iron [51]. Studies show that Cu also may exhibit somewhat Fenton-like behaviors through [52,53]:

$$Cu^{+} + H_2O_2 = Cu^{2+}\ OH\bullet + OH^{-} \quad (4)$$

$$Cu^{2+} + H_2O_2 = Cu^{+}\ O_2H\bullet + H^{+} \quad (5)$$

Thus, the influence of H_2O_2 concentration on photoelectrocatalysis of BPA was also investigated. Initial concentration values of H_2O_2 were 2.0, 5.0 and 10.0 mmol L^{-1}. As shown in Fig. 4d, at 30 min of photocalysis there was decay of absorption of BPA in all H_2O_2 concentrations studied. However, at 10 mmol L^{-1} was observed formation of

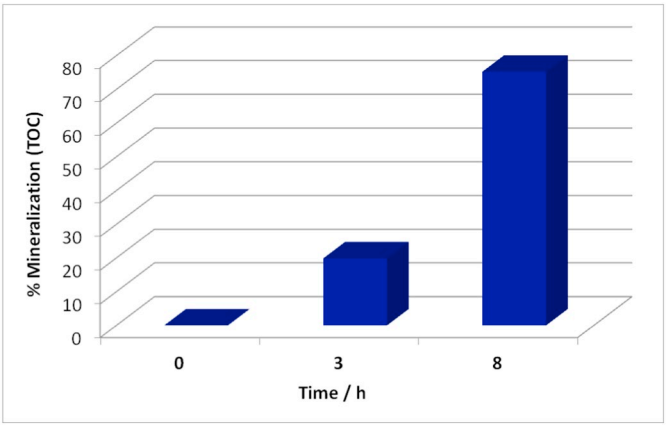

Fig. 7. BPA mineralization percentage graph in solution of 0.5 mol L^{-1} Na_2SO_4 (pH 8.0) as a function of time with photoelectrocatalysis $CW_{1.0}$ electrode (j = 10 mA cm^{-2} 10 mmol L^{-1} H_2O_2, 60 mg L^{-1} BPA, t = 8 h, vapour metallic lamp 150 W).

intermediates of reaction, since other absorption band was observed at 250 nm. In 60 min photoelectrocatalytic, there was an increase in the absorption band of the intermediates and decay of BPA absorption band with the addition of 10 mmol L^{-1} H_2O_2 (data not shown). As in this work the aim is the application of Cu doped WO_3 in BPA degradation beyond the monitoring of degradation and formation of intermediates by electrochemical methods and considering that the addition of 10 mmol L^{-1} H_2O_2 promoted greater formation of intermediates, this concentration was chosen for exhaustive photoelectrocatalysis.

3.3.2. Photoelectrochemical degradation of BPA under optimum conditions

The monitoring of BPA concentration and formation of intermediates during photocatalytic degradation experiments was made by UV–Vis spectrometry and electrochemical measurement. Experiments were performed under optimum conditions: initial BPA concentration of 60 ppm, initial pH of 8 in 0.5 mol L^{-1} of Na_2SO_4 solution, current density applied of 10 mA cm^{-2} and 10 mmol L^{-1} of H_2O_2.

Along of photoelectrolysis, aliquots were collected and diluted in Na_2SO_4 and PBS buffer solution for spectrometric and voltammetric analysis respectively. Fig. 5a shows the BPA absorption spectra during 8 h of photocatalytic treatment process. There were gradually decay absorption bands of BPA and an increase at the bands in 250 and 300 nm that can be attributed at several aromatic intermediates formation which have been reported previously in the literature. These compounds include phenol, isopropylphenol, methoxyphenol, hydroquinone, benzoquinone, catechol, glycerol, biphenyldiol, among others [54–56]. It was found 43.2% BPA was removed after 8 h of photoelectrolysis from UV–Vis spectrum. However, the intermediates formed during photoelectrolysis can have influenced at the final result. The aromatic molecules can interfere the absorption spectrum of BPA since they absorb in the same spectral region, as seen in Fig. 5b, which shows the absorption spectra of different aromatic patterns (phenol, resorcinol, catechol, hydroquinone) and of BPA. Therefore, at the condition studied, the absorption spectrometry in the UV–Vis was not recommended to monitor BPA degradation then it was used the electrochemical measurements, because this technique allows better selectivity when a suitable electrode is used [32].

The monitoring of BPA degradation by electrochemical experiments was performed using a glassy carbon electrode modified with nickel nanoparticles (NiO/MWCNT/GCE) and cyclic voltammetry (CV) such analysis technique. An apparent decrease in the current peak is observed at the cyclic voltammetry at different times of photocatalytic oxidation of BPA, Fig. 6a. Limiting the potential range of the obtained voltammograms (Fig. 6b), one can clearly see the reduction in current peak related to oxidation of BPA at 0.6 V and the formation and increase the oxidation peak around 0.2 V corresponding to the intermediates of reaction.

As discussed earlier, phenolic intermediates as hydroquinone and catechol may be formed during the oxidation of BPA. Thus, to confirm the formation of intermediate during photoelectrocatalysis experiments, cyclic voltammograms of a solution containing BPA, HQ and CC were compared with voltammogram obtained in time of 8 h of degradation, as seen in Fig. 6c. The potential of oxidation and reduction of HQ and CC at the cyclic voltammetry of the standard solution are very similar to those observed at the end of photoelectrocatalysis. Moreover, other peaks are not observed in the same oxidation potential of BPA, showing the high selectivity of electrochemical method, besides high sensitivity for monitoring BPA concentration. In less diluted samples, Fig. 6d, the initial and final voltammograms of BPA clearly show a decrease of current peak of the oxidation in 79.2%.

According to the results, it was found that monitoring the BPA concentration using electrochemical methods are more effective than spectroscopic methods, since these last, there was the interference of the intermediates formed during the oxidation of BPA.

At the end of photoelectrocatalysis (8 h), total organic carbon (TOC) was made to determine the mineralization of organic matter (Fig. 7). 75% mineralization was observed BPA after the degradation test, confirming the good performance of $CW_{1.0}$ electrode in the degradation of organic compounds.

Energy consumption (EC) to degradation of BPA was evaluated by values for EC (kWh kg^{-1}) calculated using Eq. (6) [57]:

$$Ec = \frac{i \cdot E_{cel} \cdot t}{\Delta TOC \cdot 1000} \quad (6)$$

where E_{cel} is the cell potential (V), i is the applied current (A), t is the time of photocatalysis (h) and ΔTOC is the mass of TOC removed (kg). The Ec calculated to BPA degradation was 11.73 KWh kg^{-1}. Considering that in the state of São Paulo (Brazil) the KWh costs $ 0.13, the cost of treating 1 kg of BPA is $ 1.53.

4. Conclusions

In the present study, Cu doped WO_3 electrodes were synthesized by modified sol gel method and were applied at the effective photocatalytic degradation of BPA. The monitoring of degradation was made by UV–Visible spectrometry and electrochemical measurement using a sensor NiO/MWCNT/GCE. The presence of 1% of Cu increased the photocurrent density in six times compared to WO_3 bare. The experimental conditions as initial concentration of BPA, pH, current density and H_2O_2 concentration affected significantly BPA photodegradation. The monitor of concentration of BPA during photoelectrolysis by absorbance measurements was affected due absorption of intermediates formed in same region at the spectrum at BPA. However, the monitoring the BPA concentration using electrochemical sensor was very effective and there was not interference of the reaction intermediates. After 8 h of assay, it was verified removal of 80% of BPA using electrochemical measurements and it was possible to observe the formation of intermediates by the appearance of oxidation and reduction peaks. These peaks present potential characteristic of phenolic compounds such as hydroquinone and catechol that are generally BPA degradation products. Results obtained in this study clearly demonstrate that Cu doped WO_3 electrode has potential application for photocatalysis. In addition, the electrochemical monitoring of the degradation is very effective and an alternative to conventional methods because is not observed interference of reaction intermediates of BPA.

Acknowledgments

The authors would like to thank FAPESP (Process #2012/20926-2 and #2014/10757-4), CEPID/FAPESP #2013/07296-2, FAPESP/GSK #2014/50249-8, CNPq and CAPES for the financial support.

Appendix A. Supplementary data

Supplementary data to this article can be found online at https://doi.org/10.1016/j.jelechem.2019.03.027.

References

[1] J.P. Sumpter, A.C. Johnson, Lessons from endocrine disruption and their application to other issues concerning trace organics in the aquatic environment, Environ. Sci. Technol. 39 (2005) 4321–4332, https://doi.org/10.1021/es048504a.

[2] H.G. Oliveira, L.H. Ferreira, R. Bertazzoli, C. Longo, Remediation of 17-α-ethinylestradiol aqueous solution by photocatalysis and electrochemically-assisted photocatalysis using TiO_2 and TiO_2/WO_3 electrodes irradiated by a solar simulator, Water Res. 72 (2015) 305–314, https://doi.org/10.1016/j.watres.2014.08.042.

[3] J. Sharma, I.M. Mishra, V. Kumar, Degradation and mineralization of bisphenol A (BPA) in aqueous solution using advanced oxidation processes: UV/H_2O_2 and UV/$S_2O_8^{2-}$ oxidation systems, J. Environ. Manag. 156 (2015) 266–275, https://doi.org/10.1016/j.jenvman.2015.03.048.

[4] J.H. Kang, F. Kondo, Y. Katayama, Human exposure to bisphenol A, Toxicology. 226 (2006) 79–89, https://doi.org/10.1016/j.tox.2006.06.009.

[5] R. Wang, D. Ren, S. Xia, Y. Zhang, J. Zhao, Photocatalytic degradation of bisphenol A (BPA) using immobilized TiO_2 and UV illumination in a horizontal circulating bed photocatalytic reactor (HCBPR), J. Hazard. Mater. 169 (2009) 926–932, https://doi.org/10.1016/j.jhazmat.2009.04.036.

[6] V. Likodimos, D.D. Dionysiou, P. Falaras, CLEAN WATER: water detoxification using innovative photocatalysts, Rev. Environ. Sci. Biotechnol. 9 (2010) 87–94, https://doi.org/10.1007/s11157-010-9201-z.

[7] V.M. Daskalaki, I. Fulgione, Z. Frontistis, L. Rizzo, D. Mantzavinos, Solar light-induced photoelectrocatalytic degradation of bisphenol-A on TiO_2/ITO film anode and BDD cathode, Catal. Today 209 (2013) 74–78, https://doi.org/10.1016/j.cattod.2012.07.026.

[8] P. Ju, H. Fan, S. Ai, D. Zhang, Y. Wang, Photocatalytic activity of one-dimensional $Ag_2V_4O_{11}$ nanowires in the degradation of bisphenol a under visible-light irradiation, Res. Chem. Intermed. 41 (2015) 3683–3697, https://doi.org/10.1007/s11164-013-1481-9.

[9] O. Bechambi, M. Chalbi, W. Najjar, S. Sayadi, Photocatalytic activity of ZnO doped with Ag on the degradation of endocrine disrupting under UV irradiation and the investigation of its antibacterial activity, Appl. Surf. Sci. 347 (2015) 414–420, https://doi.org/10.1016/j.apsusc.2015.03.049.

[10] J. Di, J. Xia, Y. Ge, H. Li, H. Ji, H. Xu, Q. Zhang, H. Li, M. Li, Novel visible-light-driven CQDs/Bi_2WO_6 hybrid materials with enhanced photocatalytic activity toward organic pollutants degradation and mechanism insight, Appl. Catal. B Environ. 168–169 (2015) 51–61, https://doi.org/10.1016/j.apcatb.2014.11.057.

[11] D.B. Hernandez-Uresti, D. Sánchez-Martínez, A. Martínez-de la Cruz, S. Sepúlveda-Guzmán, L.M. Torres-Martínez, Characterization and photocatalytic properties of hexagonal and monoclinic WO_3 prepared via microwave-assisted hydrothermal synthesis, Ceram. Int. 40 (2014) 4767–4775, https://doi.org/10.1016/j.ceramint.2013.09.022.

[12] R. Huang, Y. Shen, L. Zhao, M. Yan, Effect of hydrothermal temperature on structure and photochromic properties of WO_3 powder, Adv. Powder Technol. 23 (2012) 211–214, https://doi.org/10.1016/j.apt.2011.02.009.

[13] C.O. Avellaneda, L.O.S. Bulhões, Photochromic properties of WO_3 and WO_3:X (X = Ti, Nb, Ta and Zr) thin films, Solid State Ionics 165 (2003) 117–121, https://doi.org/10.1016/j.ssi.2003.08.023.

[14] G.R. Bamwenda, H. Arakawa, The visible light induced photocatalytic activity of tungsten trioxide powders, Appl. Catal. A Gen. 210 (2001) 181–191, https://doi.org/10.1016/S0926-860X(00)00796-1.

[15] X.F. Cheng, W.H. Leng, D.P. Liu, J.Q. Zhang, C.N. Cao, Enhanced photoelectrocatalytic performance of Zn-doped WO_3 photocatalysts for nitrite ions degradation under visible light, Chemosphere. 68 (2007) 1976–1984, https://doi.org/10.1016/j.chemosphere.2007.02.010.

[16] W.J. Li, Z.W. Fu, Nanostructured WO_3 thin film as a new anode material for lithium-ion batteries, Appl. Surf. Sci. 256 (2010) 2447–2452, https://doi.org/10.1016/j.apsusc.2009.10.085.

[17] M. Sadakane, K. Sasaki, H. Kunioku, B. Ohtani, W. Ueda, R. Abe, Preparation of nano-structured crystalline tungsten(VI) oxide and enhanced photocatalytic activity for decomposition of organic compounds under visible light irradiation, Chem. Commun. (Camb.) 1 (2008) 6552–6554, https://doi.org/10.1039/b815214d.

[18] S.S. Thind, M. Tian, A. Chen, Direct growth and photo-electrochemical study of WO_3 nanostructured materials, Electrochem. Commun. 43 (2014) 13–17, https://doi.org/10.1016/j.elecom.2014.03.002.

[19] D. Sánchez-Matínez, C. Gomez-Solis, L.M. Torres-Martinez, CTAB-assisted ultrasonic synthesis, characterization and photocatalytic properties of WO_3, Mater. Res. Bull. 61 (2015) 165–172, https://doi.org/10.1016/j.materresbull.2014.10.034.

[20] S.S. Thind, K. Rozic, F. Amano, A. Chen, Fabrication and photoelectrochemical study of WO_3-based bifunctional electrodes for environmental applications, Appl. Catal. B Environ. 176–177 (2015) 464–471, https://doi.org/10.1016/j.apcatb.2015.04.033.

[21] R. Abe, H. Takami, N. Murakami, B. Ohtani, Pristine simple oxides as visible light driven photocatalysts: highly efficient decomposition of organic compounds over platinum-loaded tungsten oxide, J. Am. Chem. Soc. 130 (2008) 7780–7781, https://doi.org/10.1021/ja800835q.

[22] M. Qamar, M.A. Gondal, Z.H. Yamani, Removal of Rhodamine 6G induced by laser and catalyzed by Pt/WO_3 nanocomposite, Catal. Commun. 11 (2010) 768–772, https://doi.org/10.1016/j.catcom.2010.02.012.

[23] S. Sun, W. Wang, S. Zeng, M. Shang, L. Zhang, Preparation of ordered mesoporous Ag/WO_3 and its highly efficient degradation of acetaldehyde under visible-light irradiation, J. Hazard. Mater. 178 (2010) 427–433, https://doi.org/10.1016/j.jhazmat.2010.01.098.

[24] Q. Xiang, G.F. Meng, H.B. Zhao, Y. Zhang, H. Li, W.J. Ma, J.Q. Xu, Au nanoparticle modified WO_3 nanorods with their enhanced properties for photocatalysis and gas sensing, J. Phys. Chem. C 114 (2010) 2049–2055, https://doi.org/10.1021/jp909742d.

[25] T. Arai, M. Yanagida, Y. Konishi, Y. Iwasaki, H. Sugihara, K. Sayama, Efficient complete oxidation of acetaldehyde into CO_2 over $CuBi_2O_4/WO_3$ composite photocatalyst under visible and UV light irradiation, J. Phys. Chem. C 111 (2007) 7574–7577.

[26] Z. Liu, Z.-G. Zhao, M. Miyauchi, Efficient visible light active $CaFe_2O_4/WO_3$ based composite photocatalysts: effect of interfacial modification, J. Phys. Chem. C 113 (2009) 17132–17137, https://doi.org/10.1021/jp906195f.

[27] S.A.K. Leghari, S. Sajjad, F. Chen, J. Zhang, WO_3/TiO_2 composite with morphology change via hydrothermal template-free route as an efficient visible light photocatalyst, Chem. Eng. J. 166 (2011) 906–915, https://doi.org/10.1016/j.cej.2010.11.065.

[28] T. Arai, M. Yanagida, Y. Konishi, Y. Iwasaki, H. Sugihara, K. Sayama, Promotion effect of CuO co-catalyst on WO_3-catalyzed photodegradation of organic substances, Catal. Commun. 9 (2008) 1254–1258, https://doi.org/10.1016/j.catcom.2007.11.012.

[29] H. Irie, S. Miura, K. Kamiya, K. Hashimoto, Efficient visible light-sensitive photocatalysts: grafting Cu(II) ions onto TiO_2 and WO_3 photocatalysts, Chem. Phys. Lett. 457 (2008) 202–205, https://doi.org/10.1016/j.cplett.2008.04.006.

[30] T. Arai, M. Yanagida, Y. Konishi, A. Ikura, Y. Iwasaki, H. Sugihara, K. Sayama, The enhancement of WO_3-catalyzed photodegradation of organic substances utilizing the redox cycle of copper ions, Appl. Catal. B Environ. 84 (2008) 42–47, https://doi.org/10.1016/j.apcatb.2008.03.002.

[31] S.A. Alves, L.L. Soares, L.A. Goulart, L.H. Mascaro, Solvent effects on the photoelectrochemical properties of WO_3 and its application as dopamine sensor, J. Solid State Electrochem. (2016) 1–10.

[32] L.A. Goulart, L.H. Mascaro, GC electrode modified with carbon nanotubes and NiO for the simultaneous determination of bisphenol A, hydroquinone and catechol, Electrochim. Acta 196 (2016) 48–55, https://doi.org/10.1016/j.electacta.2016.02.174.

[33] M. Deepa, T.K. Saxena, D.P. Singh, K.N. Sood, S.A. Agnihotry, Spin coated versus dip coated electrochromic tungsten oxide films: structure, morphology, optical and electrochemical properties, 51 (2006) 1974–1989, https://doi.org/10.1016/j.electacta.2005.06.027.

[34] S. Mohammadi, M. Sohrabi, A. Nozad, A. Fakhri, Preparation and characterization of zinc and copper co-doped WO_3 nanoparticles: application in photocatalysis and photobiology, J. Photochem. Photobiol. B 161 (2016) 217–221, https://doi.org/10.1016/j.jphotobiol.2016.05.020.

[35] J. Liu, J. Jin, J. Luo, X. Li, L. Zan, T. Peng, Brookite TiO_2 quasi nanocubes decorated with Cu nanoclusters for enhanced photocatalytic hydrogen production activity, Mater. Today Chem. 1–2 (2016) 23–31.

[36] P. Pongwan, K. Wetchakun, S. Phanichphant, N. Wetchakun, Enhancement of visible-light photocatalytic activity, Res. Chem. Intermed. 42 (2016) 2815–2830, https://doi.org/10.1007/s11164-015-2179-y.

[37] S. Singhal, J. Kaur, T. Namgyal, R. Sharma, Cu-doped ZnO nanoparticles: synthesis, structural and electrical properties, Phys. B Phys. Condens. Matter. 407 (2012) 1223–1226, https://doi.org/10.1016/j.physb.2012.01.103.

[38] S. Adhikari, D. Sarkar, H.S. Maiti, Synthesis and characterization of WO_3 spherical nanoparticles and nanorods, Mater. Res. Bull. 49 (2014) 325–330, https://doi.org/10.1016/j.materresbull.2013.08.028.

[39] B. Choudhury, M. Dey, A. Choudhury, Defect generation, d-d transition, and band gap reduction on Cu-doped TIO_2 nanoparticles, Int. Nano Lett. 3 (2013) 25.

[40] H. Cu, N.A.R. Materials, I. Environments, Hybrid Cu_xO/TiO_2 nanocomposites as risk-reduction materials in indoor, ACS Nano 6 (2012) 1609–1618.

[41] Y.P. Xie, G. Liu, L. Yin, H. Cheng, Crystal facet-dependent photocatalytic oxidation and reduction reactivity of monoclinic WO_3 for solar energy conversion, J. Mater. Chem. 22 (2012) 6746–6751, https://doi.org/10.1039/c2jm16178h.

[42] R. Jain, M. Shrivastava, Photocatalytic removal of hazardous dye cyanosine from industrial waste using titanium dioxide, J. Hazard. Mater. 152 (2008) 216–220, https://doi.org/10.1016/j.jhazmat.2007.06.119.

[43] V.M. Daskalaki, Z. Frontistis, D. Mantzavinos, A. Katsaounis, Solar light-induced degradation of bisphenol-A with TiO_2 immobilized on Ti, Catal. Today 161 (2011) 110–114, https://doi.org/10.1016/j.cattod.2010.09.018.

[44] S. Kaneco, M.A. Rahman, T. Suzuki, H. Katsumata, K. Ohta, Optimization of solar photocatalytic degradation conditions of bisphenol A in water using titanium dioxide, J. Photochem. Photobiol. A Chem. 163 (2004) 419–424, https://doi.org/10.1016/j.jphotochem.2004.01.012.

[45] S. Yoshihara, M. Murugananthan, Decomposition of various endocrine-disrupting chemicals at boron-doped diamond electrode, Electrochem. Commun. 54 (2009) 2031–2038, https://doi.org/10.1016/j.electacta.2008.07.006.

[46] P. Ju, H. Fan, D. Guo, X. Meng, M. Xu, S. Ai, Electrocatalytic degradation of bisphenol A in water on a Ti-based PbO_2-ionic liquids (ILs) electrode, Chem. Eng. J. 179 (2012) 99–106, https://doi.org/10.1016/j.cej.2011.10.065.

[47] S. Tanaka, Y. Nakata, T. Kimura, M. Kawasaki, H. Kuramitz, Electrochemical decomposition of bisphenol A using Pt/Ti and SnO_2/Ti anodes, J. Appl. Electrochem. 32 (2002) 197–201.

[48] Y. Cui, X. Li, G. Chen, Electrochemical degradation of bisphenol A on different anodes, Water Res. 43 (2009) 1968–1976, https://doi.org/10.1016/j.watres.2009.

01.026.
[49] Zaviska François, P. Drogui, J.-F. Blais, G. Mercier, Electrochemical treatment of bisphenol-A using response surface methodology, J. Appl. Electrochem. 42 (2012) 95–109, https://doi.org/10.1007/s10800-011-0376-y.
[50] J. Araña, C.F. Rodríguez, O.G. Díaz, J.A.H. Melián, J.P. Peña, Role of Cu in the Cu-TiO_2 photocatalytic degradation of dihydroxybenzenes, Catal. Today 101 (2005) 261–266, https://doi.org/10.1016/j.cattod.2005.03.006.
[51] V. Cleveland, J.P. Bingham, E. Kan, Heterogeneous Fenton degradation of bisphenol A by carbon nanotube-supported Fe_3O_4, Sep. Purif. Technol. 133 (2014) 388–395, https://doi.org/10.1016/j.seppur.2014.06.061.
[52] X. Zhang, Y. Ding, H. Tang, X. Han, L. Zhu, N. Wang, Degradation of bisphenol A by hydrogen peroxide activated with $CuFeO_2$ microparticles as a heterogeneous Fenton-like catalyst: efficiency, stability and mechanism, Chem. Eng. J. 236 (2014) 251–262, https://doi.org/10.1016/j.cej.2013.09.051.
[53] E. Brillas, M.A. Banos, S. Camps, C. Arias, P.-L. Cabot, J.A. Garrido, R.M. Rodriguez, Catalytic effect of Fe^{2+}, Cu^{2+} and UVA light on the electrochemical degradation of nitrobenzene using an oxygen-diffusion cathode, New J. Chem. 28 (2004) 314–322, https://doi.org/10.1039/B312445B.
[54] H. Katsumata, S. Kawabe, S. Kaneco, T. Suzuki, K. Ohta, Degradation of bisphenol A in water by the photo-Fenton reaction, J. Photochem. Photobiol. A Chem. 162 (2004) 297–305, https://doi.org/10.1016/S1010-6030(03)00374-5.
[55] H. Widiyandari, A. Purwanto, R. Balgis, T. Ogi, K. Okuyama, CuO/WO_3 and Pt/WO_3 nanocatalysts for efficient pollutant degradation using visible light irradiation, Chem. Eng. J. 180 (2012) 323–329.
[56] M. Inoue, Y. Masuda, F. Okada, A. Sakurai, I. Takahashi, M. Sakakibara, Degradation of bisphenol A using sonochemical reactions, Water Res. 42 (2008) 1379–1386.
[57] R.S. Rocha, F.L. Silva, R.B. Valim, W.R.P. Barros, J.R. Steter, R. Bertazzoli, M.R.V. Lanza, Effect of Fe^{2+} on the degradation of the pesticide profenofos by electrogenerated H_2O_2, J. Electroanal. Chem. 783 (2016) 100–105, https://doi.org/10.1016/j.jelechem.2016.11.038.